AGU PUBLICATIONS

JGR

Journal of Geophysical Research: Atmospheres

RESEARCH ARTICLE
10.1002/2015JD024712

Key Points:
- Local anisotropic ground conductivity significantly affects the arrival angle of ELF waves
- The error in ELF direction estimates varies with the azimuth of the source and the time of the day
- The dominant error term at NCK is related to variations of the conductance in the Earth's crust

Correspondence to:
J. Bór,
jbor@ggki.hu

Citation:
Bór, J., B. Ludván, N. Attila, and P. Steinbach (2016), Systematic deviations in source direction estimates of Q-bursts recorded at Nagycenk, Hungary, *J. Geophys. Res. Atmos.*, *121*, doi:10.1002/2015JD024712.

Received 23 DEC 2015
Accepted 6 MAY 2016
Accepted article online 9 MAY 2016

Systematic deviations in source direction estimates of Q-bursts recorded at Nagycenk, Hungary

József Bór[1], Brigitta Ludván[2], Novák Attila[1], and Péter Steinbach[2,3]

[1]Research Centre for Astronomy and Earth Sciences, Geodetic and Geophysical Institute, Hungarian Academy of Sciences, Sopron, Hungary, [2]Department of Geophysics and Space Sci., Geophysics, Eötvös Loránd University, Budapest, Hungary, [3]MTA-ELTE Research Group for Geology, Geophysics and Space Sciences, Budapest, Hungary

Abstract Q-bursts are globally detectable extremely low frequency (ELF, 3–3000 Hz) band wave packets produced by intense lightning discharges. Q-bursts recorded in the Széchenyi István Geophysical Observatory (NCK, 16.7°E, 47.6°N), Hungary, on 1 and 2 August 2012 have been analyzed to find azimuths of their sources. The location of parent lightning strokes of 320 and 205 Q-bursts on the 2 days, respectively, have been identified in the records of the World Wide Lightning Location Network (WWLLN) using the detection times at NCK. ELF data-based source azimuths were found to differ systematically from source azimuths obtained from WWLLN lightning locations. The difference between the corresponding azimuth values depends on the azimuth of the source. This variation of the source azimuth error mirrors the symmetry of the conductance of the Earth's crust inferred from magnetotelluric measurements around NCK. After correction for the azimuthal dependence, the variation of the residual error shows a diurnal pattern with positive azimuth deviations occurring near midnight, local time. Füllekrug and Sukhorukov (1999) suggested that the anisotropic conductivity in the Earth's crust below the observatory and the different daytime and nighttime conductivities in the lower ionosphere, respectively, may cause the identified error terms. Our results emphasize the substantial effect of anisotropic conductivity in the Earth's crust around the recording station on the accuracy of ELF direction finding. The need for theoretical approach and more measurements is pointed in understanding the underlying mechanisms quantitatively and in investigating whether ELF observations can be used in geophysical prospecting.

1. Introduction

This study was inspired by the report of *Füllekrug and Sukhorukov* [1999]. These authors have compared the directions of lightning strokes deduced from two independent data sets. On one hand, the directions were calculated from lightning stroke coordinates provided by regional lightning detection networks and from the coordinates of given extremely low frequency (ELF, 3–3000 Hz) observation sites. Directions obtained this way were used as reference. On the other hand, source directions were inferred from the orientation of the polarization plane of the horizontal magnetic component of high-amplitude ELF electromagnetic transients, i.e., Q-bursts [*Ogawa et al.*, 1966; *Nickolaenko et al.*, 2010] which had been produced by the lightning discharges and were recorded at the considered ELF observation site. The authors found that ELF data-based source directions differ from the corresponding reference directions. Two main components of the azimuth differences (or bearing errors) were identified: a term showing diurnal variation and a static term which may depend on the true source azimuth. The diurnally varying error component was shown to be caused by the anisotropic conductivity of the lower ionosphere. The horizontal rotation dependency of the other component, on the other hand, was attributed to the anisotropic conductivity in the Earth's crust in the vicinity of the observation site.

We adopted the method of *Füllekrug and Sukhorukov* [1999] to study how conductivity variations in the boundaries of the Earth-ionosphere waveguide may affect the accuracy of single-site source direction finding at the ELF recoding site near Nagycenk, Hungary (NCK). The emphasis in this study has been put on the investigation of the effect due to the varying conductivity in the Earth's crust. While most models of ELF/VLF signal propagation consider the Earth as a homogeneous medium that has infinite conductivity [*Barr et al.*, 2000; *Nickolaenko and Hayakawa*, 2002], Barr and Helm have showed [*Barr and Helm*, 1982; *Barr*, 1987] and modeled [*Barr*, 1992] how finite surface conductivities affect the propagation of VLF waves. Wait formulated methods to incorporate the finite ground connectivity in calculation of the attenuation of VLF [*Wait*, 1960a] and ELF [*Wait*, 1992] waves. *Mackay and Fraser-Smith* [2011] successfully accommodated Wait's concept to evaluate the detection efficiency of a recording station for ELF/VLF sferics propagating over regions of

different ground conductivities. Recently, *Silber et al*. [2015] have discussed the possible role of local conductivity anomalies in detections of unexpectedly high energy in the vertical magnetic component of ELF/VLF signals coming from distant sources.

The distribution of conductance in the Earth's crust at and near NCK station, inferred from magnetotelluric surveying, is characteristically uneven [*Nemesi et al*., 2000]. This study aims at examining the possible effect of this local conductivity anomaly on the polarization of ELF waves which is directly used to find the direction of their source. Compared to the work of *Füllekrug and Sukhorukov* [1999], lightning strokes occurring all around the Earth rather than only those relatively near the ELF station were considered. Lightning data used as ground truth have been provided by the World Wide Lightning Location Network (WWLLN) [*Hutchins et al*., 2012].

2. Data Used in the Present Study

2.1. ELF Time Series Recorded at NCK

The ELF recording system at NCK is part of the Széchenyi István Geophysical Observatory [*Wesztergom and Szendrői*, 2007; *Sátori et al*., 2013]. Time series of the east-west and north-south components of the magnetic field (H_{EW} and H_{NS}, respectively) as well as the vertical component of the electric field (E_Z) are recorded quasi-continuously in ~ 20 s data blocks separated by data gaps of a few milliseconds. The vertical electric component of the atmospheric electromagnetic field is measured with a capacitive ball antenna. Two induction coils carefully aligned to the geographic east-west and north-south directions are applied to detect the variation of the horizontal magnetic field. Recorded time series have UTC time stamps provided by a GPS clock. The effective bandwidth of the system is the 5–30 Hz frequency range. Regarding the data used in this study, signals in the three data channels are sampled sequentially at 514.28 Hz per channel, so that the sampling interval is ~ 1.95 ms in each time series.

2.2. Lightning Data From WWLLN

The sources of the considered ELF emissions are intense lightning discharges occurring worldwide. A lightning detection network was required which has global coverage and provides homogeneous and accurate information on the occurrences of such lightning strokes so that the available occurrence time and source coordinates can be used as ground truth data in the present study. WWLLN meets these criteria [*Rodger et al*., 2006; *Rudlosky and Shea*, 2013]. The network achieves global coverage by processing wideband VLF records quasi-real time from 50 sensors distributed worldwide (http://wwlln.net). WWLLN, as cooperation of independent institutions, is not standardized in recording bandwidths. The upper border of the bandwidth of the receivers in the network can be different at different stations. It is 24 kHz in most cases, but one can find higher and lower limits, e.g., 48 kHz or 16 kHz, too. The time-of-arrival method is used to calculate the time of occurrence and the geographical location of the source of the detected signals with microsecond and 10 km average accuracy, respectively. Wideband data in the time domain are processed centrally. Since the maximum emitted power of a lightning discharge falls in the VLF band (~10 kHz), higher frequency components of waveforms, as well as the occurring different receiver bandwidths, have no significant effect on the result.

It must be noted that the WWLLN system is known to have low detection efficiency regarding individual lightning flashes when compared to local or regional lightning detection networks operating in the MF/HF range [*Abarca et al*., 2010]. This limitation, however, is mostly valid to weak discharges. WWLLN is expected to detect more efficiently the intense lightning discharges which radiate significantly also in the ELF band and produce Q-bursts. The magnitude of Q-burst signals detected at large distances from the source scales with the vertical current moment of the source discharge. Therefore, positive polarity cloud-to-ground strokes are the most effective sources of ELF transients, because they neutralize charge centers laying generally at greater heights in the cloud and possess longer vertical discharge channels as well as stronger and longer lasting electric currents than average negative strokes [*Nickolaenko and Hayakawa*, 2002, chap. 3.1]. Unfortunately, WWLLN does not provide information either on the peak current or on the type (CG/IC) of the source, so its event listing also includes many lightning strokes which cannot be associated with Q-bursts.

2.3. Telluric Conductance Map of West Hungary

Telluric currents appear as a result of electromagnetic waves which penetrate into the Earth's crust. The strength of telluric currents depends on the frequency of electromagnetic waves and on the resistivity of

the underlying crust. The possibility of using telluric currents for geophysical exploration is based on the correct mathematical-physical description of telluric-magnetotelluric phenomena [*Tikhonov*, 1950; *Cagniard*, 1953]. Surveying of the conductivity anomalies in Earth's crust in large regions of Europe by magnetotelluric methods in various frequency bands has been started in the second half of the twentieth century [*Rokityansky*, 1982, chap. 7].

Research on telluric currents in Hungary began with the construction of measuring instruments, and the first field experiments started more than a half century ago [*Kántás*, 1954]. Systematic mapping of Transdanubia, i.e., the western part of Hungary, was conducted between 1960 and 1994 and was supported by the oil industry. The measurements initially consisted in deep penetration DC soundings, magnetotelluric, and transient observations [*Nagy et al*., 2000]. Relative measurements were carried out in a quasi-grid of several thousands of locations [*Ádám and Verő*, 1964]. The final map was compiled by translating and merging smaller relative conductivity maps using about 30 base level values from absolute conductivity measurements [*Ádám and Verő*, 1967]. During its evaluation, the telluric map was compared to previously constructed gravity and magnetic maps and to geological depth-to-the-basement maps of the pre-Tertiary basement created primarily from well data and seismic measurements. The validity of the applied methods has been confirmed by later measurements of vertical conductivity profiles across tectonically important areas in the Transdanubian region [*Nagy et al*., 2000].

The map shows effective conductance values. The effective conductance at each measuring point has been compiled from conductance values measured in two perpendicular horizontal directions. In each direction, the conductance is obtained from the geometric mean of the apparent *E* and *H* polarization resistivities at the specified period [*Nemesi et al*., 2000].

The telluric map is equivalent to a map which is derived from uniform 25 s quasi-coherent absolute telluric data. The conductances were determined at the base stations for the period of 25 s, and those values were used in the transformation of the relative telluric values. The choice of the period 25 s is supported by the fact that this period is in the middle of the range 20 to 30 s used in about 90% of stations.

Considering an average resistivity of 10 Ωm of the underlying sediments in the Earth's crust, the penetration depth of electromagnetic waves, in case of $T = 25$ s period, is 8 km. Taking into account the variation of the ambient electromagnetic field, conductance values represent the integrated property of the Earth's crust down to at most 6–8 km. Layers of higher conductance contribute more to the integral value. In the Transdanubian region, this telluric conductance map mainly reflects the effects of Tertiary-Quaternary Cenozoic sediments at depths 2000–3000 m. The conductance values are proportional to the thickness of these sediments. Note, however, that anomalously high conductivity within the underlying pre-Tertiary basement is prevalent in some localized regions. In those cases the deduced conductance values are dominated by the contribution of deeper rocks (4000–8000 m, e.g., Mesozoic carbonates) [*Nemesi et al*., 2000].

3. Data Selection and Preprocessing

3.1. Finding Q-Bursts

The days 1 and 2 August 2012 were selected for the presented analysis. On these days, the overall noise level of ELF records at NCK station was generally low, and a lot of lightning strokes were reported by WWLLN (582501 and 571595 strokes on 1 and on 2 of August, respectively).

Waveforms of Q-bursts occurring on the chosen days in the ELF time series recorded at NCK were looked up by visual inspection in the first place. The following conditions were checked in order to find Q-bursts: (1) signal peak(s) of the ELF transient must explicitly stand out from the background signal level and (2) such high-amplitude signals must occur coherently in the time series of the vertical electric field component and at least in one of the time series of the recorded magnetic field components (Figure 1). ELF transients were looked up initially in the E_Z data channel where the signal-to-noise ratio (SNR) was the highest. As a rule of thumb, transients with peak values exceeding approximately 3 times the background noise level were selected. In at least one of the more noisy magnetic data channels, the peak SNR was above two in all events. Note that from the complex Q-burst waveforms [*Nickolaenko et al*., 2010], only the peak corresponding to the signal arriving the first at the detection site was selected because the SNR is the highest for this peak. After thorough checking, 712 and 534 peaks were registered on 1 and 2 August, respectively.

The registered ELF events were processed further to deduce the direction of their source. First of all, the frequency-dependent amplitude and phase shifts due to the transmission properties of the detection system needed to be corrected [*Yatsevich et al*., 2014]. The amplitude and phase response functions of the system at NCK are not exactly the same for the electric and for the magnetic channels, so the coherency of incoming signals can be accurately evaluated only after correcting for their effects. In order to find the azimuth of the sources of the ELF transients, the method based on the evaluation of the horizontal components of the Poynting vector [*Huang et al*., 1999; *Greenberg and Price*, 2004] has been adopted. Using the Poynting vector in direction finding has more advantages compared to purely magnetic signal-based techniques [e.g., *Füllekrug and Sukhorukov*, 1999]. The SNR is higher, and the 180° uncertainty of source direction is readily resolved on the great circle path connecting the source and the observer.

The time series of the horizontal components of the Poynting vector were calculated from the system's response-corrected time series of the recorded field components as $P_{NS} = E_Z \cdot H_{EW}$, and $P_{EW} = -E_Z \cdot H_{NS}$ (Figure 1). Then, an ellipse was fitted [*Fitzgibbon et al*., 1999] to 11 points of the Poynting vector at its peak, i.e., to the point of maximum amplitude and 5-5 additional points before and after it. At the applied sampling rate, these points belonged exclusively to the considered signal peak and had the largest signal-to-noise ratio. The longer axis of the fitted ellipse determined the great circle path (GCP) passing through the source and the detection site, and the direction on this path opposite to the excursion of the peak of the Poynting vector gave the estimate of the source azimuth.

Out of the set of suspected Q-bursts, 158 (22%) and 101 (19%) events on 1 and 2 of August, respectively, had to be excluded mostly because the signals saturated one or more of the data channels, and hence, the direction estimates were biased. A fraction of the excluded events, on the other hand, were discarded because of inconsistent signal processing results. Despite the average occurrence rate of Q-bursts is only a few per minute [*Nickolaenko et al*., 2010], simultaneous detection of different Q-bursts happens because of the clusterization of lightning strokes [*Ondrásková et al*., 2008; *Yair et al*., 2009]. Overlapped ELF transients were easily identified by their nonregular pattern in the hodogram of the horizontal Poynting vector components.

3.2. Assigning Lightning Strokes to Q-Bursts

Potential parent lightning strokes of the remaining ELF transients were looked up in the WWLLN lightning database considering their location, time of occurrence, and direction at NCK station. During the lookup of the Q-burst candidates, time points of the selected signal peaks in the E_Z channel were noted. The detection time of a Q-burst at NCK station was approximated by subtracting the average time delay caused by the recording system's electronics in the E_Z data channel (23 ms) from the noted time point. This noted time point was the point having the largest absolute value in the E_Z time series corresponding to the Q-burst. If a lightning stroke occurred before the detection time of a Q-burst by at most the time ELF signals need to travel half the GCP, it can be a candidate source discharge of that Q-burst. The average propagation speed of ELF waves was assumed to be $0.8\,c$ where c is the speed of light in vacuum [*Chapman et al*., 1966]. At this speed, ELF waves need about 83 ms to travel half the circumference of the Earth. The time window we used for selecting the candidate strokes from the WWLLN database, however, was wider than this. In order to safely allow for lower signal propagation speeds, the start of the time window was set 50 ms earlier. The time window, on the other hand, was extended by 20 ms to consider the timing inaccuracy due to the system's transfer function. As a result, the time window extended 133 ms before and 20 ms after the assumed Q-burst detection time.

After that, the azimuth of each selected lightning stroke at NCK was calculated. Azimuths were deduced using the geographical coordinates of NCK station and those of the lightning strokes. These azimuth values were considered as true source directions in this study. Although ELF data-based source azimuth values are, in fact, expected to differ from the true azimuths, the differences are anticipated not to be larger than ±90°. That is, the Poynting vector in the horizontal plane is supposed to have a component parallel to the GCP at NCK which points away from its source. Lightning strokes not fulfilling this condition were not further considered.

Finally, the expected detection time of the candidate lightning strokes at NCK station was calculated. The time it takes for the ELF signals to reach NCK station from each candidate lightning stroke location on the corresponding GCP was calculated using the assumed average propagation speed of ELF waves. The expected detection time of each preselected lightning stroke was obtained by adding the calculated propagation time to its occurrence time. Generally, that lightning stroke was associated with a Q-burst for which

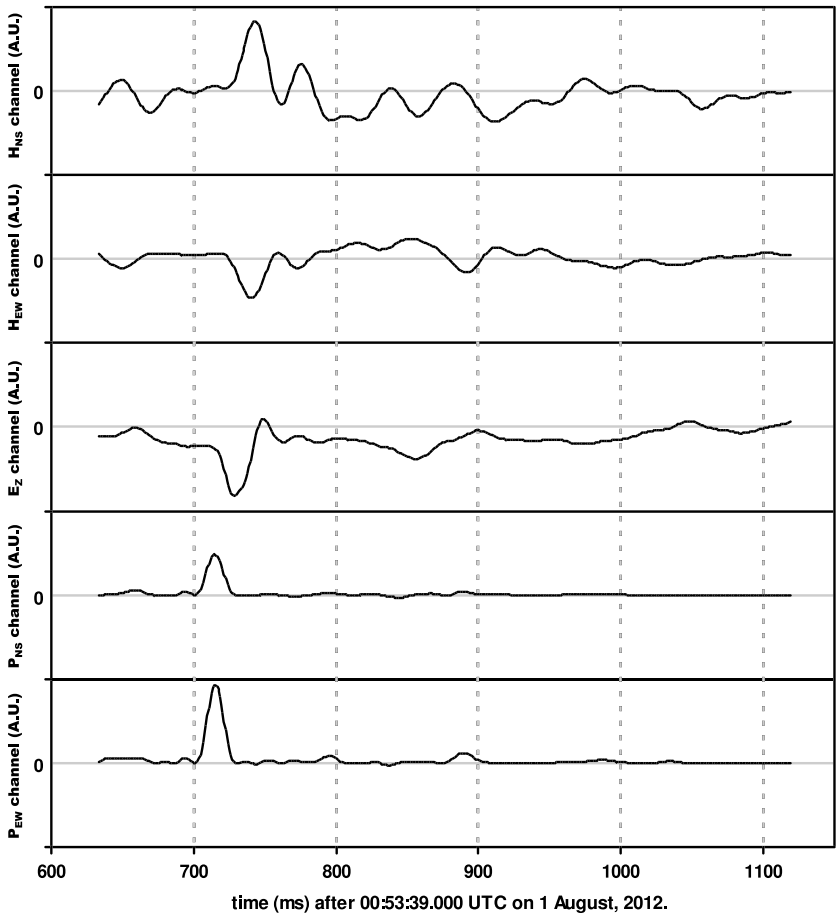

Figure 1. Raw time series and the corresponding horizontal components of the Poynting vector of a Q-burst recorded at NCK station between 00:53:39.633 and 00:53:40.120 UTC on 1 August 2012.

the expected detection time fell the closest to the considered detection time of the Q-burst. If, however, the expected detection times of more strokes were close both to the Q-burst detection time and to each other (within ±10 ms, i.e., 5 data samples), the stroke corresponding to the smallest ELF azimuth deviation was selected. By applying this procedure, a source lightning stroke from the WWLLN database could be associated to 362 and 245 Q-bursts on 1 and 2 of August, respectively.

3.3. Excluding Outlier Values

The counts of Q-bursts having an associated lightning stroke were not very high so additional conditions were introduced to compile a data set which yields more consistent results in a statistical analysis. First, the distribution of time differences between the measured and the expected detection times of Q-bursts was considered. In the majority of the cases this time difference was around +15 ms (Figures 2a and 2b). Only those events were taken further for which the time difference belonged to the main lobe of the distribution of time differences, and the number of detected cases for the given time difference was at least 5. The assignment of source lightning strokes to the rest of the Q-bursts is not convincing, so these were chosen to be left out from the presented analysis.

The bulk of azimuth deviations of the accepted events was within the ±40° range (Figure 2c). Those few events falling outside this range were excluded from the final data set. During the analysis, the considered events were binned, and the average azimuth deviation was calculated in each bin. Outliers can bias the average azimuth deviation value severely if the set of considered values is small. Drawing the limits of accepted bearing deviations at ±40° was found to be a good compromise for including most of the events and getting rid of more extreme values at the same time.

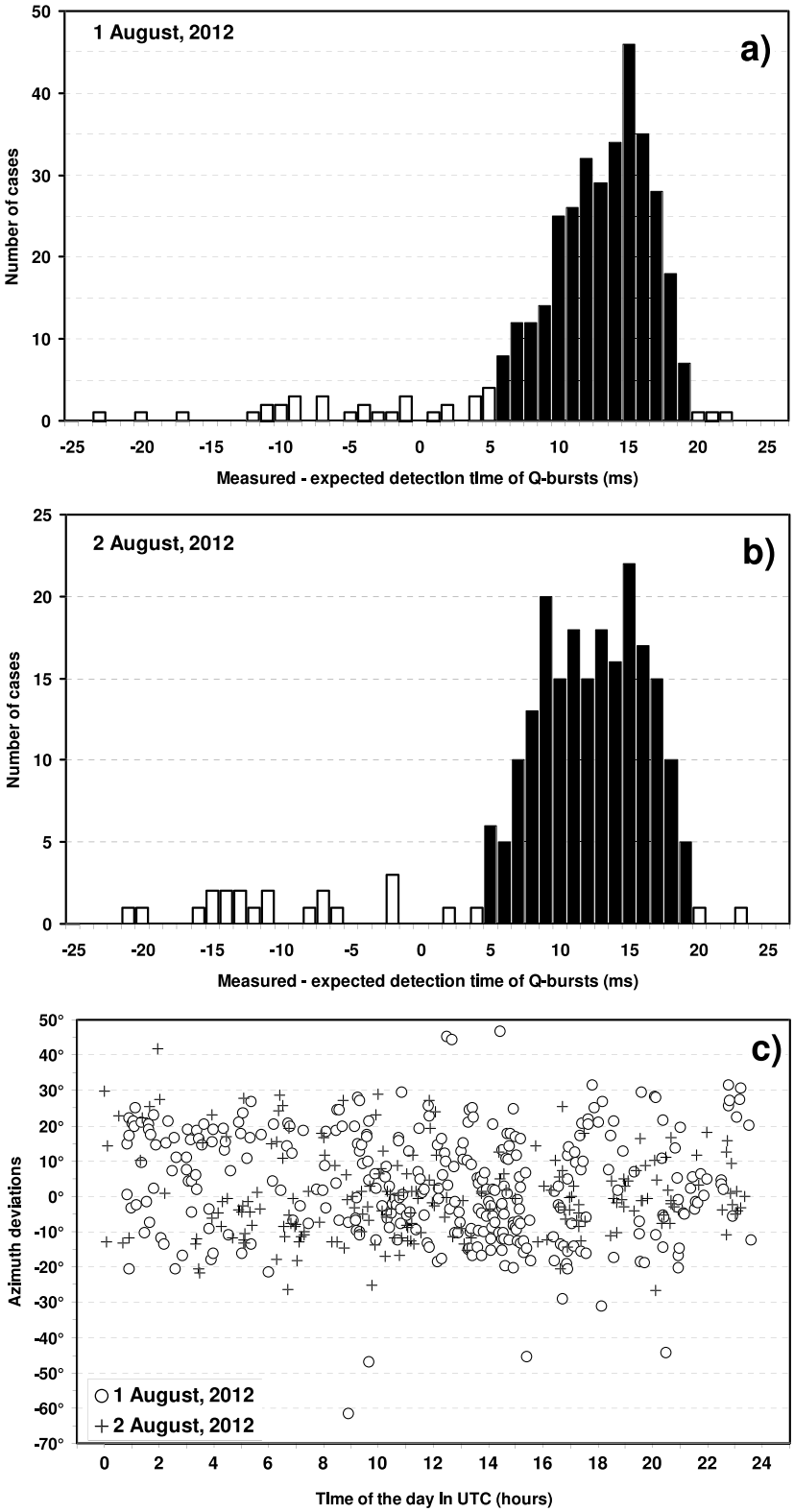

Figure 2. Distribution of the differences between the measured and the expected detection times (see text) of Q-bursts found on (a) 1 and (b) 2 August 2012. Bars of accepted time differences are filled. Average time differences corresponding to the set of accepted events is 13.2 ms and 12.3 ms on 1 and 2 August, respectively. (c) Deviation of ELF data-based source azimuths from the true azimuths (see text) for events having an accepted time differences. Azimuth deviations are plotted as a function of UTC time of their detection on the actual day.

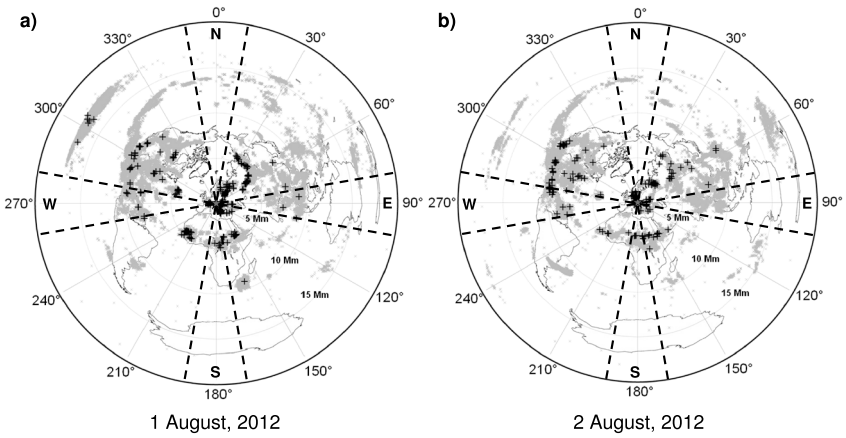

Figure 3. Global distribution of lightning strokes (cross) reported by WWLLN on (a) 1 and (b) 2 August 2012. The view is centered at NCK station (marked by a star). Concentric rings mark points of equal distances from NCK station. Points along each ray are in the same azimuth from NCK station. The edge of each plot corresponds to a single point, i.e., the geographical antipode of NCK station in the Pacific Ocean. Lightning strokes producing a Q-burst which was identified at NCK station are marked by plus signs. Dashed lines and capital letters denote azimuth sectors where the uncertainty of ELF data-based source direction finding is higher because of the finite signal-to-noise ratio in the recorded time series (see section 5 for details).

In the end, 320 and 205 Q-burst events on 1 and 2 August, respectively, remained in the data set on which the presented analysis has been carried out. Figure 3 shows the global distribution of the lightning strokes reported by WWLLN on the considered days. Lightning strokes producing a detected Q-burst at NCK station are highlighted.

4. Results

4.1. Variation of the Bearing Deviation in Terms of the True Source Azimuth

In order to see whether any variation of the ELF data-based azimuth deviation can be found in terms of the true source direction, azimuth deviations having similar true source azimuths were collected and averaged in different periods of each considered day. On both days, 2 h long overlapping time periods were considered. These time periods were centered at each whole hour from 01:00 to 23:00 UTC. Q-bursts occurred inside each of these periods were further sorted into 40° wide overlapping bins of true source azimuths. These bins were centered by 20° starting at 0°. The length of the periods and the size of the bins were defined by taking into account the limited number of events in the available data set. The calculated average azimuth deviations are shown in Tables 1 and 2 corresponding to 1 and 2 August 2012, respectively.

Average deviations in the azimuth bins were averaged further over all time periods to deduce the general variation of the ELF data-based azimuth deviations in terms of the source direction. The results are plotted on Figures 4a and 4b for 1 and 2 August, respectively. Although the azimuth deviations averaged in different periods of the day scatter significantly in each azimuth bin, the general variation of the azimuth deviation can be recognized well. On 1 August, the standard deviation (σ) of the direction errors is higher in bins containing sources to the north and to the south of NCK station. On this day, σ is the lowest for signals coming from west. On 2 August, higher standard deviation can only be found for sources to the north. At the same time, the lowest σ corresponds to the set of sources falling to the east of NCK. Furthermore, the general running of the averaged curve is very much similar on both days suggesting that the variation is not occasional.

4.2. Source Direction-Specific Bearing Deviations and Crustal Conductance

Following the reasoning of *Füllekrug and Sukhorukov* [1999], it can be suspected that the azimuth deviation varies with the true direction of the source discharge because of the anisotropic conductivity of the Earth's crust near the ELF station. Conductance of the area around and below NCK station has been surveyed by magnetotelluric measurements [*Nemesi et al.*, 2000] taken at 25 s period, i.e., at 0.04 Hz. NCK station is situated in the northwestern part of Transdanubia where the basement of the Tertiary basin is known from well samplings and seismic measurements down to depths of 3–4 km. The pre-Tertiary basement is practically

Journal of Geophysical Research: Atmospheres

10.1002/2015JD024712

Table 1. Averaged Source Azimuth Deviations for Q-Bursts on 1 August 2012[a,b]

Direction Bins (deg)	Time Bins (Hours, UTC) 00:00–02:00	01:00–03:00	02:00–04:00	03:00–05:00	04:00–06:00	05:00–07:00	06:00–08:00	07:00–09:00	08:00–10:00	09:00–11:00	10:00–12:00	11:00–13:00
00°–40°	20.6° (1)	20.6° (1)		17.8° (1)	22.8° (3)	23.7° (3)	20.4° (1)	24.4° (1)	25.8° (2)	19.8° (3)	17.4° (5)	14.5° (4)
20°–60°	18.7° (7)	17.1° (11)	13.9° (8)	16.3° (6)	20.4° (7)	20.0° (7)	18.5° (4)	20.0° (5)	18.7° (10)	17.3° (8)	18.8° (6)	15.2° (9)
40°–80°	18.4° (6)	16.7° (10)	13.1° (13)	13.5° (13)	15.2° (8)	15.4° (6)	16.5° (4)	16.9° (5)	16.1° (9)	15.7° (5)	25.6° (1)	15.7° (5)
60°–100°			12.0° (5)	12.0° (8)	11.7° (4)	11.6° (2)	12.3° (1)	8.8° (1)	4.2° (2)	−0.4° (1)	5.9° (2)	5.6° (4)
80°–120°	9.5° (1)	9.5° (1)							−0.4° (1)	−2.4° (3)	1.3° (6)	3.6° (9)
100°–140°	9.5° (1)	9.5° (1)								−3.4° (3)	−5.5° (8)	−4.9° (9)
120°–160°			−3.0° (3)	−5.0° (4)	−10.8° (1)				−3.7° (2)	−3.6° (3)	−10.1° (4)	−12.1° (6)
140°–180°			−3.0° (3)	−5.0° (4)	−10.8° (1)			−6.9° (1)	−6.3° (4)	−6.1° (3)	−5.2° (1)	−7.7° (3)
160°–200°								−6.9° (1)	−8.9° (2)	−10.9° (1)	−5.2° (1)	−5.2° (1)
180°–220°												
200°–240°	21.1° (6)	19.6° (5)	17.4° (4)	19.4° (3)		8.6° (3)	7.0° (4)	7.8° (3)	14.2° (8)	13.9° (10)	11.6° (4)	
220°–260°	21.1° (6)	19.6° (5)	17.4° (4)	19.4° (3)		8.6° (3)	7.0° (4)	7.8° (3)	14.2° (8)	13.9° (10)	11.6° (4)	
240°–280°	−1.6° (4)	−1.9° (2)							4.5° (1)	0.4° (5)	−1.6° (5)	−3.3° (2)
260°–300°	−0.9° (5)	−5.4° (5)	−6.7° (4)	−0.8° (2)			−3.0° (3)	−1.3° (4)	−4.1° (5)	−3.3° (9)	−2.1° (7)	−8.0° (5)
280°–320°	−9.5° (3)	−11.8° (6)	−12.3° (8)	−8.9° (4)	−14.8° (2)	−12.1° (3)	−3.9° (4)	−2.5° (5)	−6.5° (6)	−8.1° (9)	−7.0° (6)	−6.1° (5)
300°–340°	−12.7° (3)	−13.7° (4)	−17.8° (4)	−17.0° (2)	−17.0° (3)	−14.5° (4)	−6.8° (1)	−7.3° (1)	−6.8° (2)	−8.3° (5)	−8.8° (4)	1.3° (2)
320°–360°	−7.3° (1)	−7.3° (1)			−21.5° (1)	−21.5° (1)						
340°–20°												
Time bin average	*10.2° (22)*	*8.2° (26)*	*4.8° (28)*	*7.8° (25)*	*8.5° (15)*	*8.2° (16)*	*7.6° (13)*	*7.5° (15)*	*8.1° (31)*	*4.5° (39)*	*2.2° (32)*	*1.7° (32)*

Direction Bins (deg)	Time Bins (Hours, UTC) 12:00–14:00	13:00–15:00	14:00–16:00	15:00–17:00	16:00–18:00	17:00–19:00	18:00–20:00	19:00–21:00	20:00–22:00	21:00–23:00	22:00–24:00	Daily Average
00°–40°	13.7° (7)	14.3° (8)	12.6° (3)	16.4° (1)	18.3° (5)	18.8° (6)	25.4° (2)	20.2° (2)	10.7° (1)		25.4° (2)	*18.3° (32)*
20°–60°	14.4° (11)	16.9° (13)	15.6° (8)	10.7° (3)	16.5° (11)	18.3° (13)	22.3° (5)	19.6° (7)	18.0° (6)	25.6° (1)	26.0° (4)	*17.8° (87)*
40°–80°	10.4° (9)	12.2° (13)	13.9° (9)	10.7° (3)	15.0° (6)	17.9° (7)	20.2° (3)	19.4° (5)	19.4° (5)	25.6° (1)	26.5° (2)	*15.4° (75)*
60°–100°	4.8° (9)	5.1° (13)	6.5° (7)	11.7° (1)		17.2° (1)	17.2° (1)					*7.9° (31)*
80°–120°	2.9° (9)	−0.8° (14)	−1.0° (14)	1.0° (4)		17.2° (1)	17.2° (1)					*1.4° (32)*
100°–140°	−6.3° (7)	−7.8° (11)	−6.1° (13)	−5.5° (5)								*−5.4° (29)*
120°–160°	−11.8° (12)	−11.5° (22)	−10.9° (22)	−11.5° (14)	−12.9° (10)	−12.8° (6)	−11.7° (5)	−12.9° (8)	−12.0° (5)	2.3° (1)		*−10.9° (64)*
140°–180°	−10.6° (9)	−11.4° (18)	−10.5° (19)	−11.6° (15)	−13.4° (12)	−15.4° (7)	−14.9° (6)	−12.9° (8)	−12.0° (5)	3.5° (3)	4.1° (2)	*−10.4° (62)*
160°–200°	−5.5° (1)	−5.5° (1)	−0.9° (1)	−10.8° (3)	−15.8° (2)	−31.2° (1)	−19.2° (2)	−7.2° (1)		4.1° (2)	4.1° (2)	*−8.3° (11)*
180°–220°							−7.2° (1)	−7.2° (1)	19.5° (1)	26.1° (3)	27.0° (3)	*18.7° (5)*
200°–240°	1.9° (1)	1.9° (1)			20.7° (1)	14.2° (2)	7.6° (1)		19.5° (1)	26.1° (3)	27.0° (3)	*15.6° (33)*
220°–260°	1.9° (1)	1.9° (1)			20.7° (1)	14.2° (2)	7.6° (1)		1.2° (4)	1.2° (4)		*12.7° (33)*
240°–280°	−1.4° (1)			3.9° (2)	3.9° (2)	1.7° (1)	1.7° (1)		1.9° (6)	1.9° (7)	2.1° (1)	*0.6° (21)*
260°–300°	−10.0° (3)		−14.6° (1)	−7.7° (5)	−5.9° (4)	1.7° (1)	1.7° (1)	−6.0° (5)	−3.5° (10)	−1.2° (7)	−5.3° (3)	*−4.2° (46)*
280°–320°	−4.1° (5)	−7.2° (2)	−17.2° (2)	−11.8° (5)	−11.1° (4)			−6.0° (5)	−5.1° (8)	−4.3° (4)	−9.1° (2)	*−8.2° (50)*
300°–340°	2.7° (3)	−7.2° (2)	−19.8° (1)	−6.5° (2)	−6.5° (2)							*−10.5° (23)*
320°–360°												*−14.4° (2)*
340°–20°	3.7° (2)	2.7° (3)	8.7° (2)	16.4° (1)								*6.2° (4)*
Time bin average	*1.1° (45)*	*−0.1° (61)*	*−2.5° (51)*	*−6.0° (32)*	*0.2° (30)*	*7.4° (24)*	*2.8° (15)*	*−0.1° (21)*	*1.4° (26)*	*6.1° (18)*	*14.8° (12)*	

[a]The number of events used to calculate the average in a bin is given in parenthesis.
[b]Entries with italic type are averages of all data in the corresponding time bin or direction bin. Normal type entries are, on the contrary, averages of events only in the corresponding time and direction bin.

Journal of Geophysical Research: Atmospheres

10.1002/2015JD024712

Table 2. Same as Table 1 but for 2 August 2012[a]

Direction Bins (deg)	Time Bins (Hours, UTC) 00:00–02:00	01:00–03:00	02:00–04:00	03:00–05:00	04:00–06:00	05:00–07:00	06:00–08:00	07:00–09:00	08:00–10:00	09:00–11:00	10:00–12:00	11:00–13:00
00°–40°	19.9° (5)	20.0° (3)	21.3° (2)	15.1° (1)		19.1° (6)	19.1° (6)	8.0° (2)	8.0° (2)			
20°–60°	20.8° (6)	21.3° (4)	21.8° (3)	18.3° (3)	16.8° (1)	19.1° (6)	18.9° (7)	13.1° (6)	16.1° (7)	10.9° (6)	7.8° (8)	14.1° (6)
40°–80°	25.4° (1)	25.4° (1)	23.0° (1)	19.9° (2)	16.8° (1)		17.8° (1)	15.7° (4)	19.4° (5)	10.2° (7)	7.6° (9)	12.6° (7)
60°–100°										6.4° (1)	6.4° (1)	3.3° (1)
80°–120°					1.0° (1)	1.0° (1)			−5.1° (1)	−3.0° (3)	−1.9° (2)	
100°–140°					1.0° (1)	1.0° (1)			−5.1° (1)	−3.0° (3)	−1.9° (2)	
120°–160°						−26.4° (1)	−26.4° (1)					
140°–180°				−3.8° (1)	−3.8° (1)	−22.2° (2)	−17.5° (4)	−12.7° (2)				
160°–200°				−3.8° (1)	−3.8° (1)	−18.0° (1)	−14.5° (3)	−12.7° (2)				
180°–220°												
200°–240°											11.6° (1)	11.6° (1)
220°–260°											11.6° (1)	11.6° (1)
240°–280°		0.8° (1)	−5.7° (2)	−8.4° (2)	−7.1° (3)	−8.4° (2)	1.5° (1)	5.1° (2)	1.1° (6)	−0.2° (6)	2.4° (4)	2.2° (4)
260°–300°		0.8° (1)	−5.9° (3)	−5.0° (5)	−2.3° (11)	−2.6° (14)	−3.3° (8)	−5.7° (5)	−4.5° (10)	−2.9° (12)	−3.6° (13)	−4.3° (11)
280°–320°	−13.1° (2)		−15.5° (4)	−10.7° (6)	−1.9° (9)	−2.3° (14)	−5.9° (12)	−11.5° (7)	−13.9° (6)	−8.4° (11)	−7.6° (17)	−8.7° (13)
300°–340°	−12.6° (3)		−18.5° (3)	−15.2° (5)	−9.7° (5)	−7.1° (4)	−8.6° (5)	−11.0° (5)	−14.9° (3)	−12.7° (6)	−9.9° (9)	−9.4° (6)
320°–360°	−11.7° (1)			−10.2° (2)	−8.8° (4)	−7.4° (2)		−12.8° (1)	−12.8° (1)	−16.9° (1)	−16.9° (1)	
340°–20°												
Time bin average	*9.7° (9)*	*17.2° (5)*	*−0.9° (9)*	*−3.6° (14)*	*−3.1° (19)*	*0.3° (27)*	*−0.3° (24)*	*−1.7° (18)*	*0.9° (21)*	*−1.7° (28)*	*−1.8° (34)*	*−0.2° (25)*

Direction Bins (deg)	Time Bins (Hours, UTC) 12:00–14:00	13:00–15:00	14:00–16:00	15:00–17:00	16:00–18:00	17:00–19:00	18:00–20:00	19:00–21:00	20:00–22:00	21:00–23:00	22:00–24:00	Daily Average
00°–40°												*18.2° (15)*
20°–60°	17.8° (2)	12.5° (1)	12.5° (1)		17.9° (1)	17.9° (1)		16.6° (1)	16.6° (1)			*16.1° (37)*
40°–80°	13.0° (3)	9.5° (2)	11.1° (3)	10.0° (3)	11.2° (3)	17.9° (1)		16.6° (1)	16.6° (1)			*13.2° (28)*
60°–100°	3.3° (1)	6.5° (1)	10.4° (2)	10.0° (3)	7.9° (2)							*7.7° (6)*
80°–120°				1.8° (1)	1.8° (1)					−3.2° (2)	−3.7° (4)	*−2.3° (9)*
100°–140°				1.8° (1)	−6.4° (3)	−10.6° (2)				−3.2° (2)	−3.7° (4)	*−3.8° (11)*
120°–160°				−12.0° (3)	−11.4° (5)	−10.8° (3)	−11.3° (1)		3.3° (1)	3.3° (1)	−2.1° (2)	*−9.6° (10)*
140°–180°		−3.7° (1)	−3.7° (1)	−12.0° (3)	−12.0° (3)	−11.3° (1)	−11.3° (1)	−8.1° (4)	−5.8° (5)	3.3° (1)	−2.1° (2)	*−9.3° (17)*
160°–200°		−3.7° (1)	−3.7° (1)				16.3° (1)	−1.9° (6)	−5.6° (5)	12.5° (2)	12.5° (2)	*−2.9° (13)*
180°–220°							16.3° (1)	10.5° (2)	4.6° (1)	12.5° (2)	12.5° (2)	*11.5° (4)*
200°–240°				7.2° (1)	7.2° (1)		7.4° (1)	7.4° (1)	15.0° (2)	15.0° (2)		*11.2° (5)*
220°–260°	1.4° (1)	1.4° (1)		7.2° (1)	7.2° (1)	4.7° (2)	3.0° (5)	4.0° (4)	13.3° (3)	15.0° (2)		*6.9° (11)*
240°–280°	0.7° (3)	2.3° (3)	2.2° (2)	9.2° (3)	10.3° (3)	3.8° (4)	2.5° (6)	0.6° (6)	0.4° (3)			*1.2° (33)*
260°–300°	−1.9° (5)	1.5° (3)	2.2° (2)	9.2° (3)	10.3° (3)	2.9° (2)	1.0° (3)	−3.2° (6)	−4.9° (4)	0.8° (3)	1.0° (4)	*−2.2° (66)*
280°–320°	−8.5° (7)	−9.8° (4)		−6.5° (1)	−6.0° (3)	−5.8° (2)	−4.0° (1)	−4.9° (3)	−5.3° (2)	0.8° (3)	1.0° (4)	*−7.1° (67)*
300°–340°	−12.3° (5)	−9.7° (5)	−5.7° (2)	−9.8° (2)	−6.3° (4)	−7.2° (4)	−10.4° (1)					*−10.7° (40)*
320°–360°	−11.9° (1)	−5.1° (2)	−5.7° (2)	−7.1° (5)	−4.6° (7)	−3.3° (8)	−1.4° (7)	6.1° (3)	11.0° (1)			*−5.2° (25)*
340°–20°				−5.7° (4)	−4.2° (6)	−1.5° (6)	0.1° (6)	6.1° (3)	11.0° (1)			*−1.0° (13)*
Time bin average	*−2.2° (14)*	*−2.3° (12)*	*2.8° (8)*	*−0.7° (17)*	*−1.5° (23)*	*−2.1° (18)*	*0.8° (17)*	*1.0° (20)*	*1.6° (15)*	*5.4° (10)*	*0.8° (12)*	

[a]Entries with italic type are averages of all data in the corresponding time bin or direction bin. Normal type entries are, on the contrary, averages of events only in the corresponding time and direction bin.

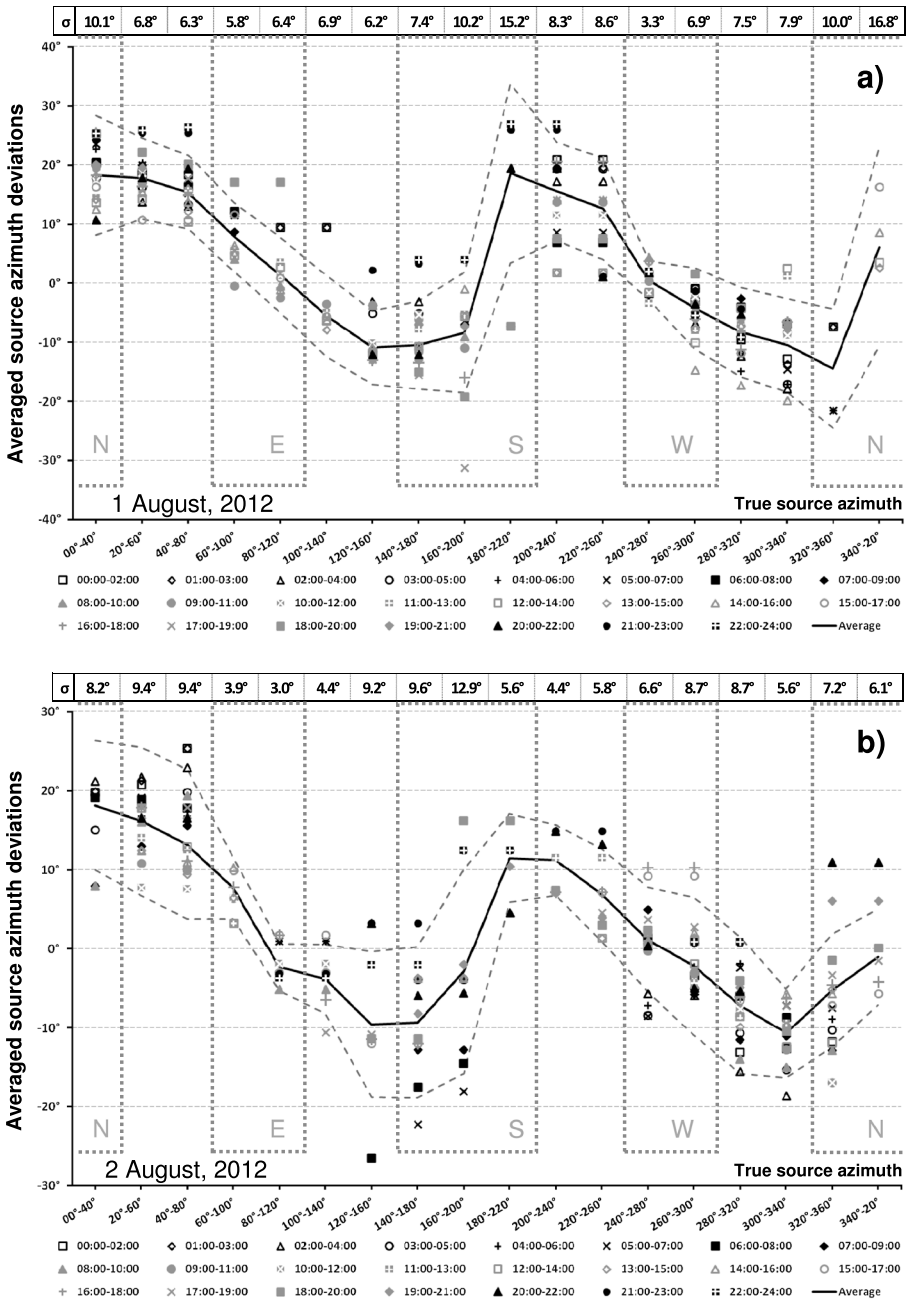

Figure 4. Averaged source azimuth deviations for Q-bursts on (a) 1 and (b) 2 August 2012. The displayed points correspond to values in Tables 1 and 2. Time ranges are in UTC. Solid curves correspond to daily averages. Dashed curves denote the $\pm\sigma$ standard deviation range around the average. Dotted rectangles border the data in bins which are possibly affected by some strokes in regions of increased source bearing uncertainty. Capital letters identify the corresponding regions on Figure 3.

at the surface to the west-northwest from NCK where lower east-alpine Palaeozoic crystalline rocks can be seen at Sopron (Figure 5). NCK station is in a local, ~2 km deep basin in the pre-Tertiary basement formed by the descending but then shortly ascending east-alpine crystalline rocks. Magnetotelluric measurements yielded anomalously high conductance values in this basin with very steep lowering toward southeast and especially toward northwest.

This variation of the conductance around NCK has been compared to the variation of azimuth deviations in terms of the true source azimuth averaged on the two considered days. The result is shown in Figure 5. A circle on the figure is centered at the location of NCK station. The diameter of this circle is 5 km which is a

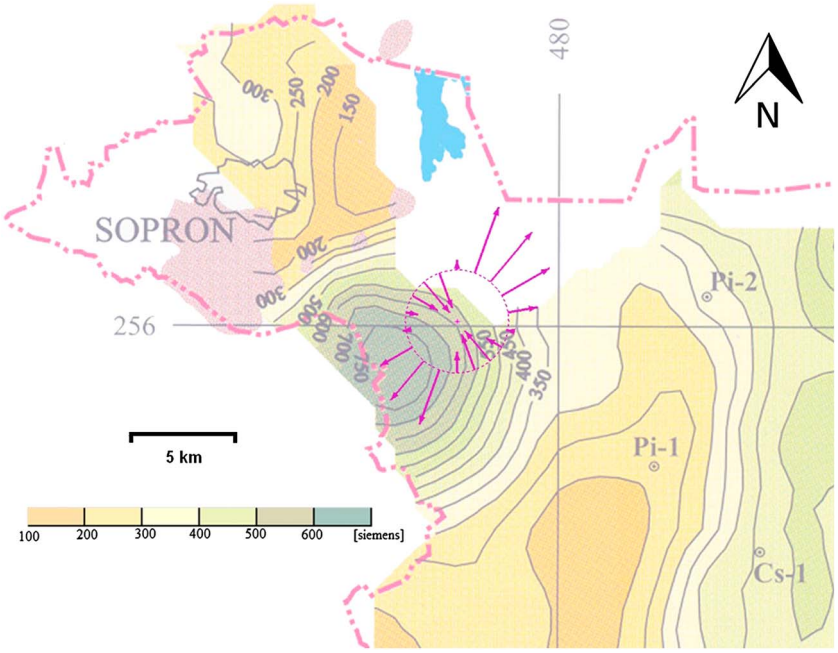

Figure 5. Conductance map [*Nemesi et al.*, 2000] near NCK station. The location of NCK station is marked by a small plus sign. Shaded area on the map shows the appearances of lower east-alpine Palaeozoic crystalline rocks at the surface near the town of Sopron. The white area without conductance data to north from NCK is part of Lake Fertő which is covered by reed. Deviations of ELF data-based source directions in terms of the true source azimuth are represented by arrows. Arrows are drawn by 20° starting at 0°. Arrows pointing inward and outward of the circle around NCK station correspond to negative and positive azimuth deviations, respectively. The length of the arrows is proportional to the absolute value of the average deviation. The length of the arrow at 20° azimuth corresponds to +18.25° azimuth deviation. See text for further details.

tentative penetration depth of 10 Hz electromagnetic waves in the Earth's crust in this region. The penetration depth of the signals was calculated by the formula $\delta \approx 0.5 \cdot \sqrt{\rho \ / f}$, where δ is the penetration depth in km, ρ is the resistivity of the Earth's crust, and f is the frequency [*Telford et al.*, 1990, pp. 306–309]. The resistivity was taken to be 1000 Ωm which is a safe upper bound for the integral resistivity of the crust in this region. Crystalline crust generally possesses resistivities greater than this value [*Schwarz*, 1990]. The penetration depth was calculated at 10 Hz because the amplitude response of the detection system is the highest at this frequency.

The pattern of average azimuth deviations apparently agrees well with the symmetry of the conductance variations around NCK.

4.3. Diurnal Variation of the Bearing Deviation

In order to be able to examine whether the variation of azimuth deviations has a diurnal component, bin averages of the azimuth deviations have been corrected by the direction-dependent component averaged for both days (the correction is explained in detail in section 4.4). The results are shown in Figure 6. Although the averages of binned values scatter significantly, a slight diurnal variation of the azimuth deviations can be recognized. Sunrise and sunset happens at around 03:30 UTC and 18:30 UTC, respectively, on the surface of the Earth at NCK station on 1 and 2 August 2015. In the lower ionosphere, daytime conditions can be assumed approximately in the 03:00–19:00 UTC period [*Sátori et al.*, 2007]. Averaged remaining azimuth deviations in time ranges corresponding to ionospheric daytime are around zero. Those azimuth deviation averages, however, which correspond to time ranges of ionospheric nighttime conditions, if not around zero, tend to be positive. This means that the average curve of azimuth deviations corrected for the source direction-dependent error component tends to show a maximum during nighttime. Considering the standard deviation of the set of values, however, this tendency is not unambiguous at NCK.

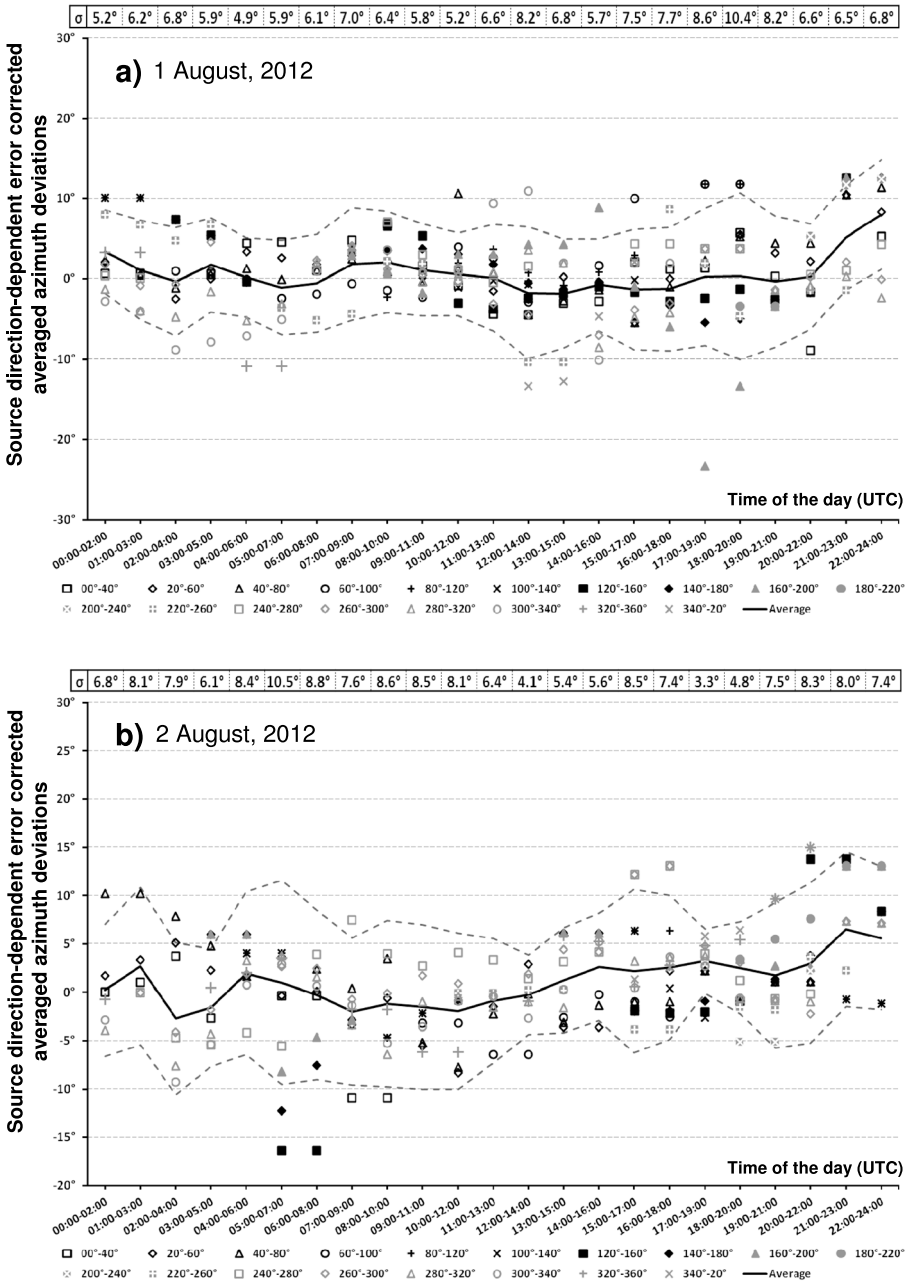

Figure 6. Daily variation of source direction-dependent error-corrected averaged azimuth deviations. Time ranges are in UTC. Solid curves correspond to values averaged over all azimuth bins. Dashed curves denote the $\pm\sigma$ standard deviation range around the average.

4.4. Remaining Error

The patterns of azimuth deviations appearing consequently in the presented statistical analysis allow examining the improvement of the ELF data-based source azimuth finding upon correction for the measured variations. Individual source azimuths from Q-burst analysis were first corrected for the source direction-dependent error term. Daily averages in each direction bin (Tables 1 and 2) were averaged for the 2 days. Interpolation was used to deduce a correction value for any true source azimuth. Correction values were then subtracted from the original ELF data-based source direction estimates. The resulting azimuths were then further corrected by the diurnal variation of the error on the corresponding day using a similar strategy. *Füllekrug and Sukhorukov* [1999] showed that the component of azimuth error which depends on the time of the day can vary significantly from day to day so we have not averaged this variation for the 2 days. Spline interpolation and extrapolation was

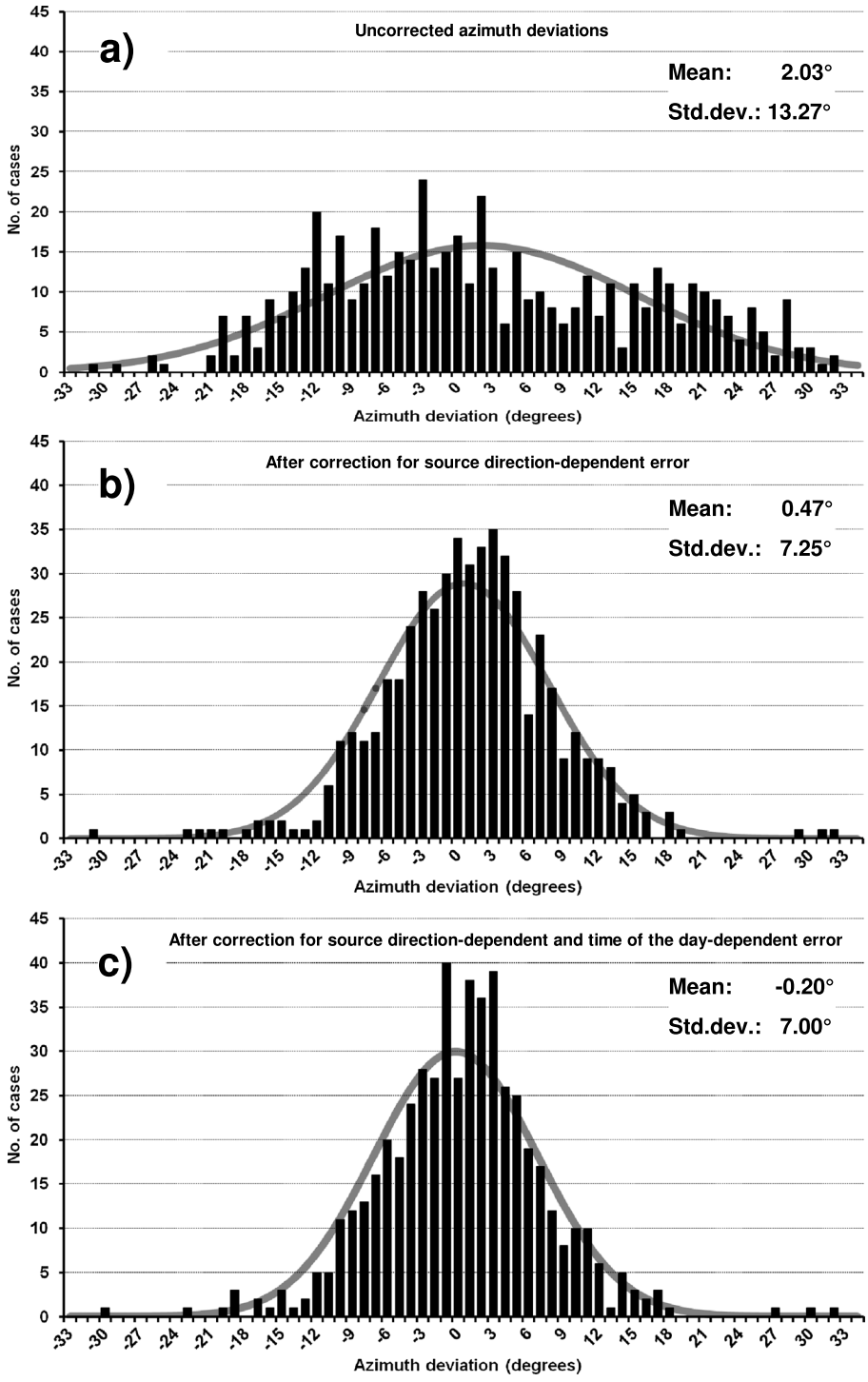

Figure 7. Distribution of deviations of all ELF data-based source azimuth estimations examined on 1 and 2 August 2012 from the WWLLN records-based true source azimuths at NCK station (a) before and (b and c) after different corrections. The curve of the fitted normal distribution is plotted in gray. Parameters of the fitted normal distribution are given on each plot.

used to calculate the correction terms at true source azimuth values and time points corresponding to the Q-burst. The results are summarized in Figure 7.

Despite the relatively low number of Q-bursts, correcting by the source direction-specific error term deduced from the data set dramatically improved the estimation of ELF data-based source direction. The additional

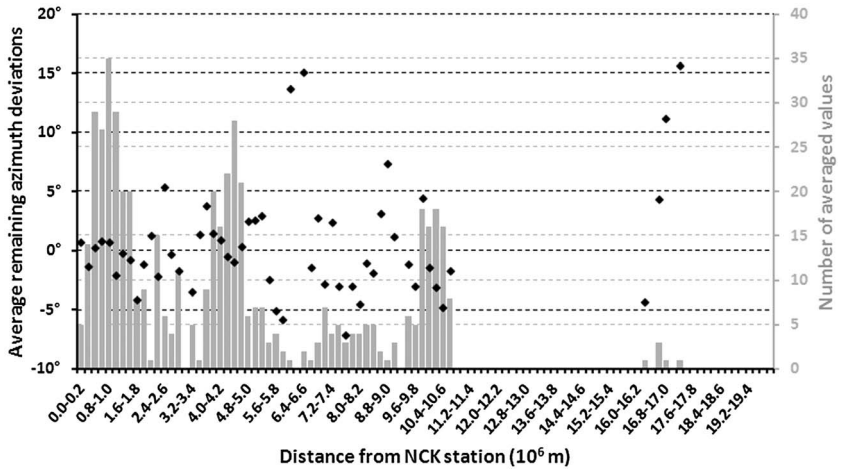

Figure 8. Variation of averaged ELF data-based source azimuth deviations corrected for both the source azimuth-specific and the daily varying error terms at NCK with the source-observer distance.

correction by the error term which depends on the time of the day has a less explicit effect; nevertheless, the main lobe of the distribution of remaining azimuth deviations becomes slightly narrower. The center of the fitted normal distribution got closer to zero, and also, the standard deviation became smaller.

4.5. Distance Dependence of the Remaining Error

ELF data-based source azimuth deviations were further examined to see whether they show any characteristic behavior in terms of the source-observer distance (SOD) after correction for both the source azimuth-specific and the daily varying error terms at NCK. Remaining azimuth deviations were sorted into bins of 0.2 Mm (=200 km) width according to their SOD. Figure 8 shows the number of averaged events in each bin as well as the average remaining direction errors.

It can be seen that the majority of considered events occurred within an 11 Mm range of NCK station. Inside this range, the average remaining deviation generally does not exceed 5° in absolute value. The remaining average error is very close to 0° for events close to NCK station and where the number of averaged events is relatively high. Larger remaining deviations occur around (6 ÷ 6.5) Mm and for events beyond 11 Mm where the number of averaged events is relatively low.

Note that the uncertainty of the true direction is expected to be higher if the source is closer to the observation station because of the limited localization accuracy of WWLLN. The localization accuracy of WWLLN depends on the density of the receiving stations in an area [*Rodger et al*., 2005]. Currently, the localization accuracy is only a few kilometers in central Europe (wwlln.net). A location error of 5 km can result in ±1.4° direction ambiguity in a distance of about 200 km. The average localization accuracy of WWLLN is approximately 10 km which causes a direction ambiguity of ±~0.6° at a source distance of about 1000 km. At greater distances the corresponding source ambiguity is lower, so this factor does not affect the results of this analysis significantly.

5. Discussion

It must be noted that only the most pronounced Q-bursts can be identified with the applied selection process, which is rather qualitative and subjective. The number of selected Q-bursts is a lower bound for the total number of Q-bursts which can be identified using more elaborated quantitative and automatic methods [*Hobara et al*., 2006, section 10.2.2.].

The peak of the distribution of time differences between the measured and the expected arrival time of Q-bursts is not at 0 ms but is shifted to + (10–15) ms (Figures 2a and 2b). Note that the detection time of a Q-burst was only roughly assigned at the selection stage (see section 3.2), and it is supposed to be closer to the peak of the pointing vector rather than to the onset time, i.e., when the signals start to rise. Therefore, the detection time in this data set corresponds approximately to the time when the most energetic part of the ELF wavefront has

passed the detection station. The generally positive time offset of the selected events in the diagrams suggests that the assumed general speed (0.8 *c*) of ELF signal propagation is overestimated. The time shift of ELF pulse propagation speeds in the 5–30 Hz frequency range are lower and can be closer to 0.7 *c* [*Chapman et al*., 1966]. Note that delayed arrival of the ELF signals can be explained partly by the difference between the time of production of the VLF and ELF radiation in the discharge process. While the VLF band radiation is dominantly produced by the return stroke, the most intense electromagnetic waves in the ELF band may originate from the subsequent continuing current phase of the lightning discharge [*Hepburn*, 1957; *Wait*, 1960b; *Reising et al*., 1996].

It can be seen in Figure 3 that eventually, no Q-burst was involved in the analysis the propagation path of which have crossed the polar regions. This may be the consequence of the increased attenuation rate of the ELF signals at high latitudes [*Burke and Jones*, 1992] but also the thunderstorm activity was not very high in the corresponding source region over the Pacific Ocean on the examined days.

The small number of Q-bursts with identified source lightning strokes at distances larger than 11 Mm (Figure 3 and 8) can be explained by the lack of intense thunderstorm activity close to the antipodal point of NCK station on the selected days and by the damped signal amplitudes in the 12–18 Mm distance range [*Nickolaenko et al*., 2008]. Events with relatively small signal amplitudes can be lost in the first stage of applied selection strategy. Furthermore, possible direction ambiguity in the Poynting vector for events near the antipodal point of the ELF station [*Ogawa and Komatsu*, 2007] can also result in dropping an event in the selection procedure.

The uncertainty of the source direction estimation is higher in those directions where the peak amplitude of the signal in a field component is below the noise level, and hence, its exact value is unknown. The affected angle range (α) around each direction the magnetic induction coils aligned to depends on the SNR as $\alpha = \arcsin(\mathrm{SNR}^{-1})$ (A. P. Nickolaenko, personal communication). In our work, horizontal components of the Poynting vector were used for direction finding. Components of the Poynting vector were deduced by multiplying the vertical electric field by the appropriate magnetic field component at each time point. The SNR of the resulting time series is thus the product of the SNRs of the used time series. From the applied selection rules, the SNR in the time series of the Poynting vector components was above 6. This means that a larger scatter of the ELF data-based direction estimates can be expected for sources in the $|\alpha| < 10°$ interval around each main geographical axis (Figure 3). The variation of the standard deviation with the source directions (Figure 4), however, does not mirror this expectation. This is partly because the selected bin size does not allow resolving this effect. On the other hand, the number of considered events is the lowest in the northern uncertainty zone (Tables 1 and 2) which contributes to the anomalously high values of standard deviation in those azimuth ranges.

Another source of direction-dependent static source azimuth error can be an asymmetry in the sensitivity pattern of either or both induction coils. Neither the design nor the environmental conditions of the antennas or the symmetry of the resulting error variations support that this factor would have a significant contribution to the azimuth errors.

Note that a variation of the azimuth deviation similar to those on Figure 4 in terms of the true source azimuth may occur also because of the improper alignment of the magnetic antennas. In such cases, the range of variation of the direction error corresponds to the deviation of the angle enclosed by the two antennas from 90°. The offset of the oscillation, on the other hand, corresponds to the negative of the anticlockwise rotation angle of the whole coordinate system taken from the geographic east-west and north-south direction. This latter shift in our case is only few degrees, while the range of the variations is 25–30°. Such large range could appear only due to a rather apparent bias in the alignments of the induction coils. Such biases do not exist at NCK station, because the magnetic antennas were aligned accurately to the main geographical axes [*Sátori et al*., 2013].

The direction-specific error term, therefore, is most probably caused by the anisotropic conductivity in the Earth's crust near NCK station. A plausible physical mechanism which causes the observed rotational symmetry in the azimuth deviations (Figure 5) remains to be found. At present it is also unclear that conductivity structures of what spatial scale can result in the observed azimuth deviations. The location of NCK station is such that the same symmetry can be found in a range of either few or few tens of kilometers around the station. If looked on a shorter scale, large positive azimuth deviations appear in source directions where the gradient of the conductance in the Earth's crust is high. If however, viewed on a larger scale, NCK station is located in a region of a saddle-like conductance variation, and large positive azimuth deviations occur in directions where the second

Table 3. Events of Remaining Azimuth Deviations Greater Than 15° in Absolute Value[a]

Date (YYYY.MM.DD)	Time (UTC)	Distance to NCK (Mm)	True Azimuth at NCK	Remaining Azimuth Deviation
2012.08.01.	00:55.05.065	10.5	306.9°	−15.0°
2012.08.01.	08:05.22.088	4.5	227.5°	−17.2°
2012.08.01.	10:22.55.344	2.4	38.1°	−15.8°
2012.08.01.	12:19.07.903	16.7	303.1°	15.2°
2012.08.01.	12:30.32.579	5.5	27.1°	−16.0°
2012.08.01.	12:59.51.061	0.5	108.8°	17.0°
2012.08.01.	13:16.16.595	1.6	18.2°	−30.1°
2012.08.01.	13:43.53.522	17.2	304.5°	15.7°
2012.08.01.	15:08.07.568	1.0	142.2°	16.9°
2012.08.01.	16:42.35.256	7.7	295.7°	−20.9°
2012.08.01.	18:06.56.326	4.7	176.2°	−23.9°
2012.08.01.	19:19.23.537	4.0	147.0°	17.9°
2012.08.02.	05:04.49.566	9.8	284.5°	31.1°
2012.08.02.	06:21.57.350	6.5	294.3°	29.7°
2012.08.02.	06:42.21.883	4.2	155.4°	−16.9°
2012.08.02.	08:51.15.144	6.0	27.8°	−19.1°
2012.08.02.	10:08.40.193	2.8	40.6°	−19.6°
2012.08.02.	10:27.34.565	10.5	56.4°	−17.1°
2012.08.02.	10:41.14.864	7.2	294.3°	16.4°
2012.08.02.	16:41.54.330	10.1	279.7°	26.1°
2012.08.02.	20:05.15.766	4.1	171.6°	−19.0°

[a]Remaining azimuth deviations are corrected for the source azimuth-specific and the daily varying error terms at NCK.

derivative of the horizontal variation of the conductance is positive. At even longer scales, Lake Fertő can play a role. The lake has relatively big open water surface to north from NCK; however, a large part of it is covered by reed very close to the ELF station (the white region toward the water on Figure 5). The symmetry of the rotational variation of the constant azimuth error, however, does not mirror that geometry.

The conductivity of the Earth's crust is known to influence the properties of atmospheric electromagnetic waves explicitly [*Barr*, 1987; *Mackay and Fraser-Smith*, 2011; *Aoki et al*., 2015]. Depending on their frequency, electromagnetic waves propagating in the Earth-ionosphere waveguide penetrate into the ground and cause currents in conductive structures. As a result, secondary electromagnetic fields are developed and added to the waves in the waveguide [*Smith*, 1995, 1997]. This effect has been, in fact, widely utilized at higher frequencies by VLF and radio magnetotelluric methods for surveying the conductivity under the Earth's surface at depths from few tens to few hundreds of meters [*McNeill and Labson*, 1991; *Bozzo et al*., 1994; *Bosch and Müller*, 2001; *Oskooi and Pedersen*, 2005; *Pedersen et al*., 2009]. Recently, the theory of interpreting spaceborne electromagnetic field measurements in order to survey conductivity in the ground has been developed. After careful removal of purely magnetospheric signals from the records, surveying techniques became available both in the VLF [*Leye and Tarits*, 2015] and in the ULF [*Civet et al*., 2015] domains. The technique described by *Civet et al*. [2015] enables the investigation of the vertical conductivity profile down to several hundreds of kilometers. The ELF domain allows making surveys in the depth range of up to few kilometers [*Tzanis and Beamis*, 1987]. This possibility has not been widely exploited so far. Additionally, the source azimuth-dependent effect discussed in this paper suggests that subsurface lateral conductivity variations might also be studied. It has been recently shown that solid knowledge on the 3-D conductivity structure of the Earth's crust is required to properly anticipate the possible electromagnetic effects of strong geomagnetic storms [*Bedrosian and Love*, 2015]. The authors, therefore, emphasize the need for a quantitative theoretical approach and more measurements in order to further confirm the findings presented in this work and to investigate whether ELF observations can be effectively used in geophysical prospecting.

The range of the average of the daily varying component of azimuth deviations at NCK was 9.8° (from −1.8° to +8.0°) and 9.2° (from −2.7° to +6.5°) on 1 and 2 of August, respectively. These ranges fairly agree with the ~10° average range of daily variation found by *Füllekrug and Sukhorukov* [1999] who studied two other ELF stations in Germany and in the United States. Note that the daily varying component was always positive at those two stations. This property was confirmed by theoretical calculations. At NCK station, however, the daily varying error term of the source azimuth estimation tends to have also negative values. This difference can be explained by a

constant error term incorporated in the daily varying error term of the ELF data-based azimuth estimations. Such term may be present due to irregular conditions in the lower ionosphere. The source of the effect causing the observed shift in the diurnal variation of the azimuth deviations at NCK remains to be identified.

In spite of the similarities and the agreement in the range of the variation of the remaining error, the diurnal variation cannot be unambiguously recognized at NCK station in the examined days. This may happen because of the actual conditions in the lower ionosphere. The diurnal variation of the remaining error showed considerable differences in the study of *Füllekrug and Sukhorukov* [1999], too.

Despite the careful selection of the events, the distribution of azimuth deviations remaining after correcting for both the source azimuth-specific and the daily varying error terms at NCK (Figure 7c) has relatively long tails. Events belonging to the tail of the distribution occurred in different times of the day and in various ranges from NCK station (Table 3). Mostly, these events are responsible for extreme values of the average remaining azimuth deviation in range bins where the number of events in the considered SOD range is low (Figure 8). The majority of the remaining azimuth deviations, however, seem to be low all day and at every SOD (at least below ~11 Mm). This suggests that the polarization of the horizontal magnetic filed component can be considerably affected also on short time scales. Conditions leading to such transient perturbations are yet to be identified.

Note that the maximum of the envelope of the histogram of azimuth deviations remaining after correcting for both the source azimuth-specific and the daily varying error terms at NCK (Figure 7c) is shifted by 2–3° to positive deviations. The reason of this offset can be the inaccuracy of the determination of the varying error terms in the ELF data-based azimuth estimation or another quasi-constant error term which does not depend on those factors which affect the daily varying error term. Unfortunately, the number of considered Q-burst is, in fact, too low to unambiguously answer this question in the framework of this study.

6. Summary and Conclusions

Statistical analysis of the deviation between ELF data-based estimations of the source azimuth of Q-bursts and the true source azimuths has confirmed that the azimuth deviation is composed of varying terms. The dominant component of the azimuth deviation at NCK varies with the direction of arrival of ELF signals. This component reflects the symmetry of conductance variations of the Earth's crust near the ELF recording station. This result indicates that not only large-scale conductivity changes like the land-ocean coast line contrast noted by *Füllekrug and Sukhorukov* [1999] but also shorter-scale conductivity variations close to the detection site in the lower boundary region of the waveguide may affect the local properties of atmospheric ELF waves.

Another component of the azimuth deviation varies with the time of the day. Slight positive or negative deviation can be noticed in the ELF data-based azimuth estimation when there are nighttime or daytime conditions, respectively, in the lower ionosphere above NCK ELF monitoring station. Neither the diurnal variation of the average azimuth deviations nor that of the standard deviation of the direction errors show statistically significant differences between daytime and nighttime conditions at NCK on the examined days. Nevertheless, the range of the diurnal variation observed in this work agrees with that found in an independent study. This range, however, seems to be shifted to lower values at NCK compared to theoretical values [*Füllekrug and Sukhorukov*, 1999]. The origin of this shift remains to be identified.

The observed general zero trend in ELF data-based azimuth deviations remaining after correction for both the source azimuth-specific and the daily varying error terms at NCK for events up to 11 Mm SOD in this study indicates that the findings of *Füllekrug and Sukhorukov* [1999] are valid also for those ELF signals which have propagated global distances before their detection. This implies that the origin of deduced components of azimuth deviations must be a local effect rather than a propagation effect.

Correction for the identified terms of error greatly improves the accuracy of ELF data-based raw source azimuth estimation. This results in more reliable localization of the sources of Q-bursts in single-site detections [*Burke and Jones*, 1995; *Huang et al*., 1999; *Greenberg and Price*, 2004].

Further studies are suggested in order to quantify, scale, and model the effect of conductivity anisotropies in the Earth's crust on ELF waves propagating over a given region in the Earth-ionosphere waveguide.

Acknowledgments

The authors wish to thank A.P. Nickolaenko for the useful comments which helped improving this paper. This work was supported by the National Research, Development and Innovation Office, Hungary-NKFIH, K115836. Contribution of József Bór was supported by the János Bolyai Research Scholarship of the HAS and by the TAMOP-4.2.2.C–11/1/KONV-2012-0015 (Earth-system) project sponsored by the EU and European Social Foundation. The authors wish to thank the World Wide Lightning Location Network (http://wwlln.net), collaboration among over 50 universities and institutions, for providing the lightning location data used in this paper. Scientific discussion related to the subject of the paper has been facilitated by the TEA-IS programme of ESF. The data used to produce the results in this paper are available upon request from the authors.

References

Abarca, S. F., K. L. Corbosiero, and T. J. Galarneau Jr. (2010), An evaluation of the Worldwide Lightning Location Network (WWLLN) using the National Lightning Detection Network (NLDN) as ground truth, *J. Geophys. Res.*, *115*, D18206, doi:10.1029/2009JD013411.

Ádám, A., and J. Verő (1964), Results of the regional telluric measurements in Hungary [in German], *Acta Tech.*, *47*(1–2), 63–77.

Ádám, A., and J. Verő (1967), Investigation of the processing telluric survey data in the case of superposition of variation with various periods [in Hungarian], *Geophys. Trans.*, *16*(1–2), 17–24.

Aoki, M., Y. Baba, and V. A. Rakov (2015), FDTD simulation of LEMP propagation over lossy ground: Influence of distance, ground conductivity, and source parameters, *J. Geophys. Res. Atmos.*, *120*, 8043–8051, doi:10.1002/2015JD023245.

Barr, R. (1987), The diffraction of VLF radio waves by the Antarctic ice cap, *J. Atmos. Solar Terr. Phys.*, *49*(1), 1–5, doi:10.1016/0021-9169(87)90075-4.

Barr, R. (1992), A simple theoretical model of the diffraction of VLF electromagnetic waves by the Antarctic icecap, *J. Atmos. Solar Terr. Phys.*, *54*(11–12), 1527–1533, doi:10.1016/0021-9169(92)90160-M.

Barr, R., and P. O. Helm (1982), Standing waves in VLF transmissions produced by geographical discontinuities, *J. Atmos. Solar Terr. Phys.*, *44*(11), 967–971, doi:10.1016/0021-9169(82)90061-7.

Barr, R., D. Llanwyn Jones, and C. J. Rodger (2000), ELF and VLF radio waves, *J. Atmos. Solar Terr. Phys.*, *62*(17–18), 1689–1718, doi:10.1016/S1364-6826(00)00121-8.

Bedrosian, P. A., and J. J. Love (2015), Mapping geoelectric fields during magnetic storms: Synthetic analysis of empirical United States impedances, *Geophys. Res. Lett.*, *42*, 10,160–10,170, doi:10.1002/2015GL066636.

Bosch, F. P., and I. Müller (2001), Continuous gradient VLF measurements: A new possibility for high resolution mapping of karst structures, *First Break*, *19*, 343–350, doi:10.1046/j.1365-2397.2001.00173.x.

Bozzo, E., S. Lombardo, and F. Merlanti (1994), VLF prospecting: Observations about field experiments, *Ann. Geofis.*, *37*(5), doi:10.4401/ag-4168.

Burke, C. P., and D. L. Jones (1992), An experimental investigation of ELF attenuation rates in the Earth-ionosphere duct, *J. Atmos. Solar Terr. Phys.*, *54*(3–4), 243–250, doi:10.1016/0021-9169(92)90005-6.

Burke, C. P., and D. L. Jones (1995), Global radiolocation in the lower ELF frequency band, *J. Geophys. Res.*, *100*(D12), 26,263–26,271, doi:10.1029/95JD02735.

Cagniard, L. (1953), Basic theory of the magneto-telluric method of geophysical prospecting, *Geophysics*, *50*, 605–635.

Chapman, F. W., D. Llanwyn Jones, J. D. W. Todd, and R. A. Challinor (1966), Observation on the propagation constant of the Earth-ionosphere Waveguide in the frequency band 8 kc/s to 16 kc/s, *Radio Sci.*, *1*(11), 1273–1282, doi:10.1002/rds19661111273.

Civet, F., E. Thébault, O. Verhoeven, B. Langlais, and D. Saturnino (2015), Electrical conductivity of the Earth's mantle from the first Swarm magnetic field measurements, *Geophys. Res. Lett.*, *42*, 3338–3346, doi:10.1002/2015GL063397.

Fitzgibbon, A., M. Pilu, and R. B. Fisher (1999), Direct least square fitting of ellipses, *IEEE Trans. Pattern Anal. Mach. Intell.*, *21*(5), 476–480, doi:10.1109/34.765658.

Füllekrug, M., and A. I. Sukhorukov (1999), The contribution of anisotropic conductivity in the ionosphere to lightning flash bearing deviations in the ELF/ULF range, *Geophys. Res. Lett.*, *26*(8), 1109–1112, doi:10.1029/1999GL900174.

Greenberg, E., and C. Price (2004), A global lightning location algorithm based on the electromagnetic signature in the Schumann resonance band, *J. Geophys. Res.*, *109*, D21111, doi:10.1029/2004JD004845.

Hepburn, F. (1957), Atmospheric waveforms with very lowfrequency components below 1 kc/s known as slow tails, *J. Atmos. Terr. Phys.*, *10*, 266–287, doi:10.1016/0021-9169(57)90125-3.

Hobara Y., M. Hayakawa, E. Williams, R. Boldi, E. Downes (2006), Location and electrical properties of sprite-producing lightning from a single elf site, in *Sprites, Elves and Intense Lightning Discharges*, *NATO Science Series II. Mathematics, physics and chemistry*, edited by M. Füllekrug, E. A. Mareev, and M. J. Rycroft, vol. 225, pp. 211–235, Springer, Verlag, doi:10.1007/1-4020-4629-4_10.

Huang, E., E. Williams, R. Boldi, S. Heckman, W. Lyons, M. Taylor, T. Nelson, and C. Wong (1999), Criteria for sprites and elves based on Schumann resonance observations, *J. Geophys. Res.*, *104*(D14), 16,943–16,964, doi:10.1029/1999JD900139.

Hutchins, M. L., R. H. Holzworth, C. J. Rodger, and J. B. Brundell (2012), Far-field power of lightning strokes as measured by the World Wide Lightning Location Network, *J. Atmos. Oceanic Technol.*, *29*, 1102–1110, doi:10.1175/JTECH-D-11-00174.1.

Kántás, K. (1954), The results of perspectives of the Hungarian telluric research [in Hungarian], *Bányász. Lapok*, *87*, 17.

Leye, P. O., and P. Tarits (2015), VLF waves at satellite altitude to investigate Earth electrical conductivity, *Radio Sci.*, *50*, 264–281, doi:10.1002/2014RS005532.

Mackay, C., and A. C. Fraser-Smith (2011), World coverage for single station lightning detection, *Radio Sci.*, *46*, RS0M01, doi:10.1029/2010RS004600.

McNeill, J. D., and V. F. Labson (1991), Geological mapping using VLF radio fields, in *Electromagnetic Methods in Applied Geophysics: Part B Application*, edited by M. N. Nabighian, pp. 521–640 , SEG, Tulsa.

Nagy, Z., L. Nemesi, and J. Verő (2000), History of telluric exploration in Trasdanubia, *Geophys. Trans.*, *43*(3–4), 121–135.

Nemesi, L., G. Varga, and A. Madarasi (2000), Telluric map of Transdanubia, *Geophys. Trans.*, *43*(3–4), 169–204.

Nickolaenko, A. P., and M. Hayakawa (2002), *Resonances in the Earth–Ionosphere Cavity*, pp. 380 , Kluwer Academic Publishers, Dordrecht–Boston–London.

Nickolaenko, A. P., M. Hayakawa, T. Ogawa, and M. Komatsu (2008), Q-bursts: A comparison of experimental and computed ELF waveforms, *Radio Sci.*, *43*, RS4014, doi:10.1029/2008RS003838.

Nickolaenko, A. P., M. Hayakawa, and Y. Hobara (2010), Q-Bursts: Natural ELF radio transients, *Surv. Geophys.*, *31*(4), 409–425, doi:10.1007/s10712-010-9096-9.

Ogawa, T., and M. Komatsu (2007), Analysis of Q burst waveforms, *Radio Sci.*, *42*, RS2S18, doi:10.1029/2006RS003493.

Ogawa, T., Y. Tanaka, T. Miura, and M. I. Yasuhara (1966), Observations of natural ELF and VLF electromagnetic noises by using ball antennas, *J. Geomag. Geoelectr.*, *18*, 443–454.

Ondrásková, A., J. Bór, S. Sevcík, P. Kostecký, and L. Rosenberg (2008), Peculiar transient events in the Schumann resonance band and their possible explanation, *J. Atmos. Sol. Terr. Phys.*, *70*, 937–946, doi:10.1016/j.jastp.2007.04.013.

Oskooi, B., and L. B. Pedersen (2005), Comparison between VLF and RMT methods. A combined tool for mapping conductivity changes in the sedimentary cover, *J. Appl. Geophys.*, *57*, 227–241, doi:10.1016/j.jappgeo.2005.01.002.

Pedersen, L. B., L. Persson, M. Bastani, and S. Byström (2009), Airborne VLF measurements and mapping of ground conductivity in Sweden, *J. Appl. Geophys.*, *67*, 250–258, doi:10.1016/j.jappgeo.2007.11.002.

Reising, S., U. Inan, T. Bell, and W. Lyons (1996), Evidence for continuing current in sprite-producing cloud-to-ground lightning, *Geophys. Res. Lett.*, *23*, 3639–3642, doi:10.1029/96GL03480.

Rodger, C. J., J. B. Brundell, and R. L. Dowden (2005), Location accuracy of VLF World-Wide Lightning Location (WWLL) network: Post-algorithm upgrade, *Ann. Geophys.*, *23*, 277–290, doi:10.5194/angeo-23-277-2005.

Rodger, C. J., S. Werner, J. B. Brundell, E. H. Lay, N. R. Thomson, R. H. Holzworth, and R. L. Dowden (2006), Detection efficiency of the VLF World-Wide Lightning Location Network (WWLLN): Initial case study, *Ann. Geophys.*, *24*, 3197–3214, doi:10.5194/angeo-24-3197-2006.

Rokityansky, I. I. (1982), *Geoelectromagnetic Investigation of the Earth's Crust and Mantle*, p. 382, Springer, Berlin, doi:10.1007/978-3-642-61801-7

Rudlosky, S. D., and D. T. Shea (2013), Evaluating WWLLN performance relative to TRMM/LIS, *Geophys. Res. Lett.*, *40*, 2344–2348, doi:10.1002/grl.50428.

Sátori, G., M. Neska, E. Williams, and J. Szendrői (2007), Signatures of the day-night asymmetry of the Earth-ionosphere cavity in high time resolution Schumann resonance records, *Radio Sci.*, *42*, RS2S10, doi:10.1029/2006RS003483.

Sátori, G., M. Rycroft, P. Bencze, F. Märcz, J. Bór, V. Barta, T. Nagy, and K. Kovács (2013), An Overview of thunderstorm-related research on the atmospheric electric field, Schumann resonances, sprites, and the ionosphere at Sopron, Hungary, *Surv. Geophys.*, *34*(3), 255–292, doi:10.1007/s10712-013-9222-6.

Schwarz, G. (1990), Electrical conductivity of the Earth's crust and upper mantle, *Surv. Geophys.*, *11*(2), 133–161, doi:10.1007/BF01901658.

Silber, I., C. Price, E. Galanti, and A. Shuval (2015), Anomalously strong vertical magnetic fields from distant ELF/VLF sources, *J. Geophys. Res. Space Physics*, *120*, 6036–6044, doi:10.1002/2015JA021141.

Smith, J. T. (1995), Understanding telluric distortion matrices, *Geophys. J. Int.*, *122*(1), 219–226, doi:10.1111/j.1365-246X.1995.tb03549.x.

Smith, J. T. (1997), Estimating galvanic-distortion magnetic fields in magnetotellurics, *Geophys. J. Int.*, *130*(1), 65–72, doi:10.1111/j.1365-246X.1997.tb00988.x.

Telford, W. M., L. P. Geldart, and R. E. Sheriff (1990), *Applied Geophysics*, pp. 792, Cambridge Univ. Press, Cambridge.

Tikhonov, A. N. (1950), Determination of the electrical characteristics of the deep strata of the Earth's crust, *Dokl. Akad. Nauk. SSSR*, *73*, 295–297.

Tzanis, A., and D. Beamis (1987), Audiomagnetotelluric sounding using the Schumann resonances, *J. Geophys.*, *61*(2), 97–109.

Wait, J. R. (1960a), Terrestrial propagation of very-low-frequency radio waves: A theoretical investigation, *J. Res. Natl. Bur. Stand. D*, *64*(2), 153–203, doi:10.6028/jres.064D.022.

Wait, J. R. (1960b), On the theory of the slow tail portion of atmospheric wave forms, *J. Geophys. Res.*, *65*(7), 1939–1946, doi:10.1029/JZ065i007p01939.

Wait, J. R. (1992), On ELF transmission in the Earth-ionosphere waveguide, *J. Atmos. Solar Terr. Phys.*, *54*(1), 109–111, doi:10.1016/0021-9169(92)90089-4.

Wesztergom, V., and J. Szendrői (Eds.) (2007), *Geophysical Observatory Reports of the Geodetic and Geopysical Research Institute of the Hungarian Academy of Sciences, Year 2005–2006*, Special Issue on the Occasion of the 50th Anniversary of the Observatory, Geod. and Geophys. Res. Inst. of the Hungarian Acad. of Sci., Sopron, Hungary, HU-ISBN:978-963-8381-22-4, HU-ISSN 0133-459X.

Yair, Y., R. Aviv, and G. Ravid (2009), Clustering and synchronization of lightning flashes in adjacent thunderstorm cells from lightning location networks data, *J. Geophys. Res.*, *114*, D09210, doi:10.1029/2008JD010738.

Yatsevich, E. I., A. V. Shvets, and A. P. Nickolaenko (2014), Impact of ELF receiver on characteristics of ELF transients, *Radiophys. Quant. Electron.*, *57*(3), 176–186, doi:10.1007/s11141-014-9502-0.